The Astrophysical Journal Letters, 806:L17 (5pp), 2015 June 10 doi:10.1088/2041-8205/806/1/L17

ALMA RESOLVES THE PROPERTIES OF STAR-FORMING REGIONS IN A DENSE GAS DISK AT $z \sim 3$

A. M. Swinbank[1,2], S. Dye[3], J. W. Nightingale[3], C. Furlanetto[3,4], Ian Smail[1,2], A. Cooray[5], H. Dannerbauer[6], L. Dunne[7,8], S. Eales[9], R. Gavazzi[10], T. Hunter[11], R. J. Ivison[8,12], M. Negrello[13], I. Oteo-Gomez[8,12], R. Smit[1,2], P. van der Werf[14], and C. Vlahakis[15,16]

[1] Institute for Computational Cosmology, Department of Physics, Durham University, South Road, Durham DH1 3LE, UK; a.m.swinbank@dur.ac.uk
[2] Center for Extragalactic Astronomy, Department of Physics, Durham University, South Road, Durham DH1 3LE, UK
[3] School of Physics and Astronomy, Nottingham University, University Park, Nottingham NG7 2RD, UK
[4] CAPES Foundation, Ministry of Education of Brazil, Brasília/DF, 70040-020, Brazil
[5] Astronomy Department, California Institute of Technology, MC 249-17, 1200 East California Boulevard, Pasadena, CA 91125, USA
[6] Institut fur Astrophysik, Universitat Wien, Türkenschanzstrasse 17, 1180 Wien, Austria
[7] Department of Physics and Astronomy, University of Canterbury, Private Bag 4800, Christchurch 8140, New Zealand
[8] Institute for Astronomy, Royal Observatory Edinburgh, Blackford Hill, Edinburgh, EH9 3HJ, UK.
[9] School of Physics and Astronomy, Cardiff University, Queen's Buildings, The Parade, Cardiff CF24 3AA, UK
[10] Institut d'Astrophysique de Paris, UMR7095 CNRS-Universite Pierre et Marie Curie, 98bis bd Arago, F-75014 Paris, France
[11] National Radio Astronomy Observatory, 520 Edgemont Road, Charlottesville, VA, 22903, USA
[12] European Southern Observatory, Karl-Schwarzschild-Str. 2, Garching, Germany
[13] INAF, Osservatorio Astronomico di Padova, Vicolo Osservatorio 5, I-35122 Padova, Italy
[14] Leiden Observatory, Leiden University, P.O. Box 9513, NL-2300 RA Leiden, The Netherlands
[15] Joint ALMA Observatory, Alonso de Cordova 3107, Vitacura, Santiago, Chile
[16] European Southern Observatory, Alonso de Cordova 3107, Vitacura, Santiago, Chile
Received 2015 May 1; accepted 2015 May 18; published 2015 June 9

ABSTRACT

We exploit long baseline ALMA submillimeter observations of the lensed star-forming galaxy SDP 81 at $z = 3.042$ to investigate the properties of the interstellar medium (ISM) on scales of 50–100 pc. The kinematics of the ^{12}CO gas within this system are well described by a rotationally supported disk with an inclination-corrected rotation speed, $v_{\rm rot} = 320 \pm 20\,{\rm km\,s^{-1}}$, and a dynamical mass of $M_{\rm dyn} = (3.5 \pm 1.0) \times 10^{10}\,M_{\odot}$ within a radius of 1.5 kpc. The disk is gas-rich and unstable, with a Toomre parameter, $Q = 0.30 \pm 0.10$, and so into star-forming regions with Jeans length $L_{\rm J} \sim 130$ pc. We identify five star-forming regions within the ISM on these scales and show that their scaling relations between luminosity, line widths, and sizes are significantly offset from those typical of molecular clouds in local galaxies (Larson's relations). These offsets are likely to be caused by the high external hydrostatic pressure for the ISM, $P_{\rm tot}/k_{\rm B} \sim 40^{+30}_{-20} \times 10^7\,{\rm K\,cm^{-3}}$, which is $\sim 10^4\times$ higher than the typical ISM pressure in the Milky Way. The physical conditions of the star-forming ISM and giant molecular clouds appear to be similar to those found in the densest environments in the local universe, such as those in the Galactic center.

Key words: galaxies: evolution – galaxies: high-redshift – galaxies: starburst

1. INTRODUCTION

Giant molecular clouds in local galaxies follow well-known scaling relations between CO velocity line width (σ) and their physical extent, R, with $\sigma \propto R^{1/2}$, and mean molecular gas density scales and size $\langle n({\rm H_2})\rangle \propto R^{-1}$ (Larson 1981; Bolatto et al. 2008). These scalings reflect the dynamical state of the turbulent molecular gas in the interstellar medium (ISM). Since most of the stars in local, massive spheroids and elliptical galaxies appear to have formed early in the history of the universe ($z \sim 2$–3), examining the physical, dynamical, and thermal state of the molecular gas within the ISM of galaxies at this epoch acquires special importance. However, to measure the properties of individual star-forming regions requires a spatial resolution of at least ~100 pc (sufficient to resolve sizes and velocity dispersions of the most massive giant molecular clouds). To date, this has only been achieved in a few rare examples of high-redshift galaxies whose images have been gravitationally lensed by massive galaxy clusters (see, e.g., Jones et al. 2010; Livermore et al. 2012, 2015).

To test whether the scaling relations that govern the structure of local giant molecular clouds (GMCs) are valid in the dense and rapidly evolving ISM of high-redshift, gas-rich galaxies, in this Letter we exploit ALMA observations of SDP 81—a star-forming galaxy at $z = 3.042$ whose image has been gravitationally lensed by a factor $15.8 \pm 0.7\times$ by a massive, foreground ($z \sim 0.299$) galaxy (Dye et al. 2015). The combination of long baselines, together with gravitational lensing means we are able to resolve the largest giant molecular clouds within the ISM (Solomon et al. 1987; Scoville & Good 1989) on scales approaching 50 pc. We use the spatially resolved 1.0 mm (rest-frame 250 μm) continuum imaging to identify the brightest star-forming regions, and measure their sizes, luminosities, and velocity dispersions. We use a ΛCDM cosmology with $H_0 = 72\,{\rm km\,s^{-1}\,Mpc^{-1}}$, $\Omega_m = 0.27$, and $\Omega_\Lambda = 1 - \Omega_m$ (Spergel et al. 2003), and a Chabrier IMF.

2. OBSERVATIONS AND SOURCE-PLANE RECONSTRUCTION

SDP 81 was identified from the *H-ATLAS* survey as a bright submillimeter source at $z = 3.042$ by Negrello et al. (2010). Optical imaging and spectroscopy also revealed the presence of a massive foreground galaxy at $z = 0.299$ that lenses the background galaxy (Negrello et al. 2014). Observations of SDP 81 with ALMA in its long baseline configuration (up to 15 km) were taken in 2014 October. These observations and reduction are described by Vlahakis et al. (2015). Briefly, the ALMA Band 7 (1.0 mm) continuum observations have a resolution of 31×23 mas and reach a 1σ depth of 11 μ

Jy beam^{-1}. At the redshift of the galaxy, these observations sample the rest-frame 250 μm emission. Lower-frequency observations of the ^{12}CO(5-4) and continuum emission at 2.1 mm were also made, reaching a resolution of 56×50 mas.

Dye et al. (2015) construct a detailed lens model for the system using both the ALMA submillimeter and *Hubble Space Telescope* (*HST*) imaging (see also Rybak et al. 2015). The best-fit lens model suggests that the background source comprises three dominant components, a dense gas disk (that lies inside the caustic and gives rise to the bright submillimeter emission in the image plane) and two galaxy nuclei (which lie on—or just outside—the caustic), which are visible in the *HST JH*-band imaging. Dye et al. interpret the complex morphology as a merging system in which the gas disk is a result of an early stage interaction. In their model, the luminosity weighted amplification is $\mu_{\rm submm} = 15.8 \pm 0.7$ and $\mu_{\rm opt} = 10.2 \pm 0.5$ for the submillimeter and rest-frame optical emission, respectively. Thus, correcting for lensing amplification, the observed 850 μm flux density of the galaxy is $S_{850\mu{\rm m}} \sim 1.2$ mJy, which is representative of the SMG population that has recently been studied in detail, in particular with ALMA (Hodge et al. 2013; Karim et al. 2013; Simpson et al. 2014). However, the amplifications mean that the average source plane resolution is ~50–100 pc—a factor ~30 × higher than that so far achieved in the non-lensed case (see, e.g., Ikarashi et al. 2014; Simpson et al. 2015).

3. ANALYSIS AND DISCUSSION

Using the lens modeling from Dye et al. (2015), we reconstruct the source-plane morphology of SDP 81 at 1.0 mm and 2.1 mm and show these in Figure 1. The dust continuum morphology appears clumpy, and we isolate five of the brightest star-forming regions from the highest-resolution (1.0 mm) image (using the criteria that they are 5σ above the *local* background), and label these A–E. Independently, we also use the CLUMPFIND algorithm (Williams et al. 1994), which isolates clumps A–D, although it misses clump E. However, none of our conclusions significantly change if we include / exclude region E from the analysis below.

To measure the source-plane point-spread function (PSF) we reconstruct the beam in a grid of positions in the image plane and measure the PSF at each reconstructed position in the source plane. On average, the source-plane PSF has a FWHM ~60 pc (Figure 1). In Figure 1 we also show the one-dimensional 1.0 mm, 2.1 mm, and ^{12}CO(5-4) emission profiles extracted from the major morphological axis of the source. The dust continuum and ^{12}CO emission profiles are not perfectly aligned. However, at this resolution, offsets between the CO-emitting gas and continuum may be expected in regions with high star formation density where the ^{12}CO(5-4) (which traces the warm and dense gas) is shock-heated, which efficiently raises the gas temperature and density through mechanical heating, but does not heat the dust. Indeed, if the disk fragments into a number of large star-forming regions (as we discuss below), we expect large-scale shocks where the complexes interact.

In Figure 1 we also show the source-plane ^{12}CO(5-4) velocity field (see also Dye et al. 2015), which resembles a rotating system with a peak-to-peak velocity of 210 ± 10 km s^{-1} within 1.5 kpc. The best-fit disk model suggests an inclination of $\theta = 40^\circ \pm 5^\circ$ and thus a dynamical mass of $M_{\rm dyn} = (3.5 \pm 1.0) \times 10^{10}\, M_\odot$ within a radius of 1.5 kpc. The total gas mass for the disk, estimated from either the (amplification corrected) ^{12}CO(1-0) luminosity, or using the far-infrared SED and an appropriate dust-to-gas ratio is $2.7\text{–}3.9 \times 10^{10}\, M_\odot$ (Dye et al. 2015). Together these indicate that the central regions of the disk are baryon-dominated with a gas fraction of $f_{\rm gas} \sim M_{\rm gas}/M_{\rm dyn} \sim 70\%\text{–}90\%$.

The Toomre parameter Q characterizes the stability of a disk against local axisymmetric perturbations. Gas-rich disks with $Q < 1$ should fragment and collapse into star-forming regions. Numerical simulations have also suggested that tidal interactions and dynamical friction should force the resulting star-forming regions toward the center of the galaxy, where they should coalesce to form a bulge (which in turn stabilizes the disk against further collapse; see, e.g., Genzel et al. 2008; Ceverino et al. 2010). The Toomre parameter is calculated by $Q = \sigma_{\rm r}\,\kappa/\pi G \Sigma_{\rm gas}$, where $\kappa = a\, V_{\rm max}/R$ is the epicyclic frequency (with $a = \sqrt{3}$), $\sigma_{\rm r}$ is the line of sight velocity dispersion, and $\Sigma_{\rm gas}$ is the mass surface density of the gas (Toomre 1964). For SDP 81, we derive $Q = 0.30 \pm 0.10$, which is lower than typical for the gas in local ULIRGs ($Q \sim 1$; Downes & Solomon 1998), and slightly lower than the average Toomre Q of other gas-rich star-forming $z \sim 2$ galaxies ($\langle Q \rangle = 0.85 \pm 0.13$; Genzel & Förster Schreiber 2014—although their sample also extend down to comparable values, $Q = 0.18 \pm 0.02$).

This global instability will cause large, dense gas clouds to form in the molecular gas. The fragmentation of the gas occurs on scales of the Jeans length, $L_{\rm J}$ which can be estimated using the gas surface density and average gas velocity dispersion according to $L_{\rm J} = \pi\sigma_{\rm r}^2 / 8\, G\Sigma_{\rm gas}$. For SDP 81, with $\Sigma_{\rm gas} = 4 \pm 1 \times 10^9\, M_\odot$ kpc^2 and $\sigma_{\rm r} =$ 30–35 km s^{-1} we estimate $L_{\rm J} = 130^{+200}_{-60}$ pc. If the gas fragments on these scales, the corresponding masses of the clouds that form should be $\sigma_{\rm r}^4 / G^2 \Sigma_{\rm gas} \sim 1\text{–}2 \times 10^8\, M_\odot$.

Given that our source-plane resolution is at least comparable to the Jeans length, we investigate the properties of the star-forming regions on these scales. As Figure 1 shows, the disk contains several bright star-forming regions (A–E) and we measure their sizes, luminosities, and velocity dispersions (using the beam-corrected velocity dispersion map for the velocity dispersions; Davies et al. 2011). In all five regions the ^{12}CO(5-4) has intrinsic velocity dispersions of 10–35 km s^{-1} (Table 1). To estimate sizes for the molecular gas associated with these regions, we use two approaches. First, we fit the submillimeter light profile with Gaussian profiles (centered on each star-forming region; Figure 1). Second, we measure the area subtended by a contour that is 5σ above the local background. The resulting sizes (deconvolved for the source-plane PSF) are FWHM = 170–310 pc, which is comparable to the *initial* fragmentation scale. We also estimate the molecular gas mass in the vicinity of the star-forming regions using the ^{12}CO(5-4) line luminosity and account for both the local background and the ^{12}CO(1-0)/ ^{12}CO(5-4) luminosity ratio in velocity bins (see Dye et al. 2015), obtaining gas masses of $M_{\rm gas,clumps} = 1\text{–}5 \times 10^8\, M_\odot$. These masses are consistent with those derived from using their line width and sizes with $M_{\rm dyn} = C\sigma^2$ R/G with $C = 5$—as approriate for a uniform density sphere—with $M_{\rm dyn}/M_{\rm CO} = 1.5 \pm 0.5$).

In Figure 2 we compare the velocity dispersions, luminosities, and sizes of the star-forming regions in SDP 81 with similar measurements for GMCs in the local universe (compiled from observations of the Milky Way disk and other

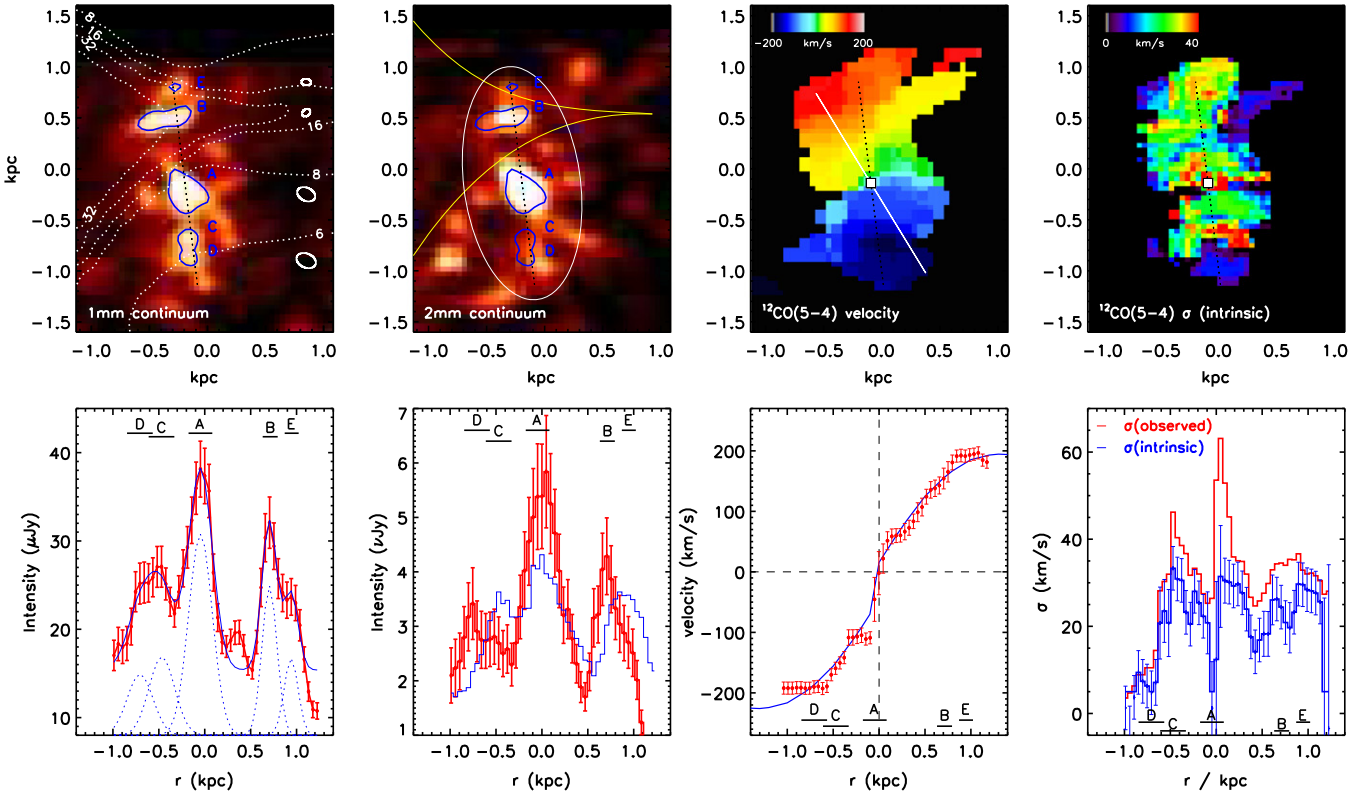

Figure 1. Source-plane images of SDP 81. Top left: source-plane 1.0 mm (rest-frame 250 μm image) continuum image of SDP 81. The star-forming clumps, A–E, are identified by the solid contours. The black dashed line defines the major morphological axis and the white contours indicate the amplification map. The luminosity weighted amplification at 1.0 mm is 16.0 ± 0.7. The white ellipses show the source-plane PSF at the location of the clumps (offset to the right-hand side of the image for clarity). Center left: source-plane 2.1 mm image with the clumps identified at 1.0 mm also highlighted. The solid line denotes the caustic curve from the best-fit lens model. Center right: ^{12}CO(5-4) velocity field. The gas disk has an observed peak-to-peak velocity gradient of 210 ± 10 km s^{-1}. The solid white line shows the major kinematic axis and the dotted line denotes the major 1.0 mm morphological axis. Top right: beam-corrected ^{12}CO(5-4) line of sight velocity dispersion. Bottom left: one-dimensional profile of the 1.0 mm continuum emission extracted across the major morphological axis. We label the five bright star-forming regions (A–E). The best-fit profiles are shown as dashed lines. Center left: one-dimensional profile of the 2.1 mm intensity extracted along the major axis of the 1.0 mm continuum with the ^{12}CO(5-4) intensity profile overlaid for comparison (blue). Center right: one-dimensional velocity profile of the gas disk with a best-fit dynamical model overlaid. Right: one-dimensional velocity dispersion profile (red) and intrinsic, beam-corrected (ΔV / Δr) velocity dispersion profile (blue). In all of the lower panels we show the positions of the star-forming regions. The source-plane submillimeter morphology appears complex / clumpy, but with the star-forming regions embedded in a dense, rotating disk.

Table 1
Clump Properties

ID	v_{clump} (km s^{-1})	Amplification (μ)	FWHM$_{clump}$ (pc)	σ_{clump} (km s^{-1})	$f_{CO(5-4)}$ (mJy km s^{-1})	r_{54}	M_{gas} ($\times 10^8$ $M_\odot$)
A	−42 ± 65	7.2 ± 0.8	282 ± 25	30 ± 9	57 ± 4	0.28 ± 0.05	1.2
B	162 ± 12	40.1 ± 1.0	188 ± 25	35 ± 3	24 ± 4	0.30 ± 0.12	2.8
C	−150 ± 28	6.2 ± 0.18	305 ± 95	31 ± 7	46 ± 4	0.28 ± 0.08	4.8
D	−176 ± 2	5.9 ± 0.15	300 ± 70	11 ± 7	35 ± 4	0.36 ± 0.05	0.8
E	204 ± 5	30.4 ± 7.4	170 ± 40	31 ± 3	28 ± 4	0.18 ± 0.04	0.7

Notes. v_{clump} denotes the velocity of the disk at the position of the star-forming region with respect to the systemic redshift. The amplifications are 1.0 mm emission luminosity weighted values. FWHM$_{clump}$ have been deconvolved for the source-plane PSF. σ_{clump} is the velocity dispersion of the clump as measured from the intrinsic ^{12}CO(5-4) velocity dispersion map. r_{54} is the ratio of the ^{12}CO(5-4)/ ^{12}CO(1-0) luminosities derived from velocity and amplification maps (Dye et al. 2015). M_{gas} denotes the gas mass of each clump assuming $M_{gas} = \alpha_{CO}\ L'_{CO(1-0)}$ with $L'_{CO(1-0)} = L'_{CO(1-0)}/r_{54}$ and $\alpha_{CO(1-0)} = M_{gas}\,/\,L'_{CO(1-0)} = 1$.

quiescent galaxies; Bolatto et al. 2008), and with the properties of GMCs and star-forming regions in more extreme environments, including the Galactic center and the ISM of SMM J2135−0102—a star-forming galaxy at $z = 2.32$ where similar measurements have been made (Swinbank et al. 2011). At a fixed size, the velocity dispersions of the star-forming regions in SDP 81 appear to be ∼4× larger than those of GMCs in quiescent environments, but more similar to those found in the Galactic center and other gas-rich environments. In the local universe, these offsets are usually attributed to high external pressures on the cloud surfaces due to high gas densities (Blitz & Rosolowsky 2004, 2006; Keto et al. 2005).

To interpret the offsets in the properties of the star-forming regions in SDP 81, we use the dynamics and surface density of the molecular gas to estimate the ISM pressure (the kinetic

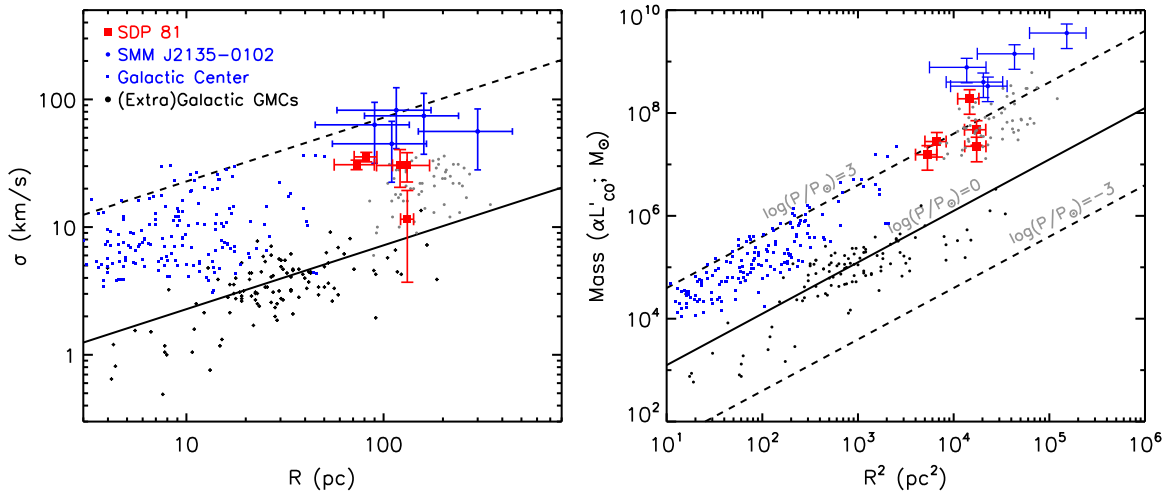

Figure 2. Relations between size, luminosity, and velocity dispersion for the star-forming regions in SDP 81 compared to those in the both quiescent and more extreme environments of the Milky Way and other local galaxies. Left: the velocity dispersion vs. cloud radius. The solid line shows the line–width–size relation for local GMCs (Larson 1981; Bolatto et al. 2008). The normalization of this scaling relation is set by the gas pressure in the disk (Elmegreen 1989). The dashed line shows the local relation but offset by a factor of 10×. GMCs in high pressure environments, such as the Galactic center (blue points) or in gas-rich galaxies such as M64 (gray points) are offsets in the sense that they have higher velocity dispersions at fixed sizes. Indeed, the star-forming regions in SDP 81 appear to have velocity dispersions that are ∼4× higher than expected. However, it is also interesting to note that their velocity dispersions are ∼2× lower than the star-forming regions in SMM J2135–0102. Right: the relation between gas mass and size; $M(\mathrm{H_2}) - R^2$. The star-forming regions in SDP 81 are again offset from those of local GMCs, and instead are consistent with having much higher luminosities at fixed sizes—a consequence of the high turbulent pressure of the ISM (see Section 3).

pressure resulting from non-ordered mass motions). In a rotating gas disk, the mid-plane hydrostatic pressure is given by

$$P_{\rm tot} \approx \frac{\pi}{2} G \Sigma_{\rm gas} \left[\Sigma_{\rm gas} + \left(\frac{\sigma_{\rm gas}}{\sigma_\star} \right) \Sigma_\star \right], \quad (1)$$

where $\Sigma_{\rm gas}$, $\Sigma_\star$, and $\sigma_{\rm gas}$, $\sigma_\star$ are the surface density and velocity dispersion of the gas and stars, respectively. In the Milky Way, $P_{\rm tot}/k_{\rm B} \sim 1.4 \times 10^4$ cm^{-3} K (Elmegreen 1989). The stellar mass of SDP 81 estimated from the rest-frame UV/optical photometry is $M_\star = (6.6^{+2.6}_{-1.9}) \times 10^{10}\, M_\odot$ (Negrello et al. 2014), although the stars appear to be offset by ∼1.5 kpc from the dust and gas emission (Dye et al. 2015), and thus we adopt $M_\star \lesssim 3 \times 10^{10}\, M_\odot$ as an upper limit on the stellar contribution within the gas disk. We also assume that the velocity dispersions of the gas and stars are comparable, $\sigma_{\rm gas}/\sigma_\star \sim 1$ (although we allow this to vary from 0.5–2 in the calculation below). Given the high gas surface density, the mid-plane hydrostatic pressure is high, $P_{\rm tot}/k_{\rm B} \sim 40^{+30}_{-20} \times 10^7$ K cm^{-3}, and although we caution that this value has considerable uncertainty, this pressure is $\gtrsim 10^4 \times$ higher than the typical pressure in the Milky Way disk (10^4 K cm^{-3}). This pressure is also ∼10× higher than inferred for the ISM in more extreme environments, such as in the Galactic center or the Antennae (Keto & Myers 1986; Wilson et al. 2003; Rosolowsky & Blitz 2005). However, the compact disks of some ULIRGs, with high gas surface densities ($\gtrsim 5 \times 10^3\, M_\odot$ pc^{-2}; Downes & Solomon 1998), may also result in comparably high pressures. Finally, we note that the implied pressure in SDP 81 is compatible with recent hydrodynamic models, which suggests that the typical pressure in the ISM of star-forming galaxies should increase from $\sim 10^4$ K cm^{-2} at $z = 0.1$ to $\sim 10^6$–10^7 K cm^{-2} at $z = 2$, reaching $\sim 10^9$ K cm^{-2} in some systems (Crain et al. 2015).

To relate the pressure to the properties of the star-forming regions, we use "Larson's relations" for turbulent molecular clouds. Following Elmegreen (1989), the velocity dispersion–size and mass–size relations can be cast as

$$\sigma = \sigma_\circ \left(\frac{P_{\rm ext}/k_{\rm B}}{10^4 \text{ K cm}^{-3}} \right)^{1/4} \left(\frac{R}{\rm pc} \right)^{1/2} \quad (2)$$

and

$$M(\mathrm{H_2}) = 290 \left(\frac{P_{\rm ext}/k_{\rm B}}{10^4 \text{ cm}^{-3} \text{ K}} \right)^{1/2} \left(\frac{R}{\rm pc} \right)^2 M_\odot, \quad (3)$$

with $\sigma_\circ = 1.2$ km s^{-1} (Larson 1981). Using Equation (2), a pressure of $10^4 \times$ that of the Milky Way therefore suggests that the velocity dispersions of the clouds within the ISM of SDP 81 should be $\gtrsim$10× those in the Milky Way, respectively (at a fixed size). The average velocity dispersion of the clumps in SDP 81 is four times larger at a fixed size than predicted from GMCs in the Milky Way, and although this is lower than the factor of 10× predicted for pressure induced offsets alone, we reiterate that this is a simplified model that nevertheless relates the offsets in the scaling relations for GMCs with the gas densities and pressures in the ISM. Finally, in Figure 2 we plot the mass–radius relation for a similar range of quiescent and extreme environments in both the Milky Way and other nearby galaxies and plot the positions of star-forming regions in SDP 81, which are again offset to higher masees by a factor ∼10× (at a fixed size) with respect to those of GMCs in quiescent environments. This can also be attributed to the high turbulent pressure (Equation (3)). However, it is interesting to note that they do not appear as massive as the star-forming regions in SMM J2135 −0102, although the latter is a natural consequence of the mass scale for collapse within the disk given their relative velocity dispersions and gas surface densities ($\sigma_{\rm SMM\ J2135}/\sigma_{\rm SDP81} \sim 2.3$ and $\Sigma_{\rm gas,SMM\ J2135}/\Sigma_{\rm gas,SDP81} \sim 2$), which results in a mass scale

difference for the clumps of $M_{\rm cl,SMMJ2135}/M_{\rm cl,SDP81} \sim 25$—consistent with Figure 1.

4. CONCLUSIONS

Using long baseline ALMA observations, we have mapped the distribution of star formation and molecular gas in the lensed, star-forming $z = 3.042$ galaxy, SDP 81, on physical scales of ~50–100 pc. The ^{12}CO(5-4) dynamics suggest that the molecular gas is located in a disk with an inclination-corrected rotation speed of $v_{\rm rot} = 320 \pm 20$ km s^{-1} and a dynamical mass of $M_{\rm dyn} = (3.5 \pm 1.0) \times 10^{10} M_{\odot}$ within a radius of 1.5 kpc.

The gas disk appears to be Toomre unstable, $Q = 0.30 \pm 0.10$. This instability will cause large, dense star-forming regions to collapse on scales of the Jeans length, $L_{\rm J} = 130^{+200}_{-60}$ pc. We identify five star-forming regions on these scales in the rest-frame 250 μm continuum and measure their sizes, luminosities, and CO velocity dispersions. We show that these star-forming regions do not lie on the local relations for GMCs, but are instead systematically offset such that the velocity dispersion is ~4× higher than typical GMCs at a fixed size.

The gas dynamics and surface density suggest that the ISM should be highly pressurized, and we estimate a mid-plane hydrostatic pressure that is ~10^4× higher than typically found in the Milky Way. These high pressures appear to be responsible for the offsets in the scaling relations of the star-forming regions compared to those of typical GMCs in galaxies in the local universe. Within the star-forming ISM of this dense gas disk, the physical conditions appear to be similar to those only seen in the densest environments in the local universe (see, e.g., Kruijssen & Longmore 2013).

We would like to thank the anonymous referee for a constructive report on this paper. A.M.S. acknowledges an STFC Advanced Fellowship (ST/H005234/1) and the Leverhume foundation. I.R.S. acknowledges STFC (ST/I001573/1), the ERC Advanced Grant DUSTYGAL 321334, and a Royal Society/Wolfson Merit Award. C.F. acknowledges CAPES funding (proc. 12203-1). We also thank Padelis Papadopoulos for useful discussions. This paper uses data from ALMA program ADS/JAO.ALMA#2011.0.00016.SV. ALMA is a partnership of ESO, NSF (USA), NINS (Japan), NRC (Canada), NSC and ASIAA (Taiwan), and KASI (Republic of Korea) and the Republic of Chile. The JAO is operated by ESO, AUI/NRAO and NAOJ.

REFERENCES

Blitz, L., & Rosolowsky, E. 2004, ApJL, 612, L29
Blitz, L., & Rosolowsky, E. 2006, ApJ, 650, 933
Bolatto, A. D., Leroy, A. K., Rosolowsky, E., Walter, F., & Blitz, L. 2008, ApJ, 686, 948
Ceverino, D., Dekel, A., & Bournaud, F. 2010, MNRAS, 404, 2151
Crain, R. A., Schaye, J., Bower, R. G., et al. 2015, MNRAS, 450, 1937
Davies, R., Förster Schreiber, N. M., Cresci, G., et al. 2011, ApJ, 741, 69
Downes, D., & Solomon, P. M. 1998, ApJ, 507, 615
Dye, S., Furlanetto, C., Swinbank, A. M., et al. 2015, MNRAS, submitted (arXiv:1503.08720)
Elmegreen, B. G. 1989, ApJ, 344, 306
Genzel, R., Burkert, A., Bouché, N., et al. 2008, ApJ, 687, 59
Genzel, R., Förster Schreiber, N. M., Rosario, D., et al. 2014, ApJ, 796, 7
Hodge, J. A., Karim, A., Smail, I., et al. 2013, ApJ, 768, 91
Ikarashi, S., Ivison, R. J., Caputi, K. I., et al. 2014, ApJ, submitted (arXiv:1411.5038)
Jones, T. A., Swinbank, A. M., Ellis, R. S., Richard, J., & Stark, D. P. 2010, MNRAS, 404, 1247
Karim, A., Swinbank, A. M., Hodge, J. A., et al. 2013, MNRAS, 432, 2
Keto, E., Ho, L. C., & Lo, K. 2005, ApJ, 635, 1062
Keto, E. R., & Myers, P. C. 1986, ApJ, 304, 466
Kruijssen, J. M. D., & Longmore, S. N. 2013, MNRAS, 435, 2598
Larson, R. B. 1981, MNRAS, 194, 809
Livermore, R. C., Jones, T., Richard, J., et al. 2012, MNRAS, 427, 688
Livermore, R. C., Jones, T. A., Richard, J., et al. 2015, MNRAS, 450, 1812
Negrello, M., Hopwood, R., De Zotti, G., et al. 2010, Sci, 330, 800
Negrello, M., Hopwood, R., Dye, S., et al. 2014, MNRAS, 440, 1999
Rosolowsky, E., & Blitz, L. 2005, ApJ, 623, 826
Rybak, M., McKean, J. P., Vegetti, S., Andreani, P., & White, S. D. M. 2015, MNRAS, in press (arXiv:1503.02025)
Scoville, N. Z., & Good, J. C. 1989, ApJ, 339, 149
Simpson, J. M., Smail, I., Swinbank, A. M., et al. 2015, ApJ, 799, 81
Simpson, J. M., Swinbank, A. M., Smail, I., et al. 2014, ApJ, 788, 125
Solomon, P. M., Rivolo, A. R., Barrett, J., & Yahil, A. 1987, ApJ, 319, 730
Spergel, D. N., Verde, L., Peiris, H. V., et al. 2003, ApJS, 148, 175
Swinbank, A. M., Papadopoulos, P. P., Cox, P., et al. 2011, ApJ, 742, 11
Toomre, A. 1964, ApJ, 139, 1217
Vlahakis, C., Hunter, T. R., Hodge, J. A., et al. 2015, ApJL, in press (arXiv:1503.02652)
Williams, J. P., de Geus, E. J., & Blitz, L. 1994, ApJ, 428, 693
Wilson, C. D., Scoville, N., Madden, S. C., & Charmandaris, V. 2003, ApJ, 599, 1049